

ASKAP and VLASS search for a radio-continuum counterpart of ultra-high-energy neutrino event KM3–230213A

M. D. FILIPOVIĆ ¹ Z. J. SMEATON ¹ A. C. BRADLEY ¹ D. DOBIE ^{2,3} B. S. KORIBALSKI ^{4,1} R. KOTHES ⁵
L. RUDNICK ⁶ A. AHMAD ¹ R. Z. E. ALSABERI ^{1,7} C. S. ANDERSON ⁸ L. A. BARNES ¹ M. BREUHAUS ⁹
E. J. CRAWFORD ¹ S. DAI ^{4,1} Y. A. GORDON ¹⁰ N. GUPTA ¹¹ A. M. HOPKINS ¹² D. LEAHY ¹³
K. J. LUKEN ¹ N. MCCLURE-GRIFFITHS ⁸ M. J. MICHAŁOWSKI ¹⁴ M. SASAKI ¹⁵ N. F. H. TOTHILL ¹
G. M. UMANA ¹⁶ T. VERNSTROM ¹⁷ AND J. WEST ¹³

¹Western Sydney University, Locked Bag 1797, Penrith South DC, NSW 2751, Australia

²Sydney Institute for Astronomy, School of Physics, University of Sydney, Sydney, NSW 2006, Australia

³ARC Centre of Excellence for Gravitational Wave Discovery (OzGrav), Hawthorn, Victoria, 3122, Australia

⁴Australia Telescope National Facility, CSIRO, Space and Astronomy, P.O. Box 76, Epping, NSW 1710, Australia

⁵Dominion Radio Astrophysical Observatory, Herzberg Astronomy & Astrophysics, National Research Council Canada, P.O. Box 248, Penticton

⁶Minnesota Institute for Astrophysics, University of Minnesota, Minneapolis, MN, 55455, USA

⁷Faculty of Engineering, Gifu University, 1-1 Yanagido, Gifu 501-1193, Japan

⁸Research School of Astronomy & Astrophysics, The Australian National University, Canberra ACT 2611, Australia

⁹Centre de Physique des Particules de Marseille, 163, avenue de Luminy, 13009 Marseille, France

¹⁰Department of Physics, University of Wisconsin-Madison, 1150 University Avenue, Madison, WI 53706, USA

¹¹CSIRO Space & Astronomy, Bentley, WA, Australia

¹²School of Mathematical and Physical Sciences, 12 Wally's Walk, Macquarie University, NSW 2109, Australia

¹³Department of Physics and Astronomy, University of Calgary, Calgary, Alberta, T2N 1N4, Canada

¹⁴Astronomical Observatory Institute, Faculty of Physics and Astronomy, Adam Mickiewicz University, ul. Słoneczna 36, 60-286 Poznań, Poland

¹⁵Dr Karl Remeis Observatory, Erlangen Centre for Astroparticle Physics, Friedrich-Alexander-Universität Erlangen-Nürnberg, Sternwartstraße 7, 96049 Bamberg, Germany

¹⁶INAF - Osservatorio Astrofisico di Catania, Via Santa Sofia 78, 95123 Catania, Italy

¹⁷Australia Telescope National Facility, CSIRO, Space and Astronomy, PO Box 1130, Bentley, WA 6102, Australia

ABSTRACT

We present the results of an Australian Square Kilometre Array Pathfinder (ASKAP) 944 MHz and Very Large Array Sky Survey (VLASS) 3 GHz search for a radio-continuum counterpart of the recent ultra-high-energy (UHE) neutrino event, KM3–230213A. Using ASKAP, we catalog 1052 radio sources within the 1.5 radius search area (68% certainty region) around the particle's calculated origin, 10 of which we classify as blazar candidates based on their radio spectra. The most prominent radio source in the search area is the nearby spiral galaxy UGCA 127 (nicknamed Phaedra^a). Its non-thermal radio spectrum classifies it as a non-blazar active galactic nucleus (AGN). We also present an extended radio source, WISEA J061715.89–075455.4 (nicknamed Hebe^b), located only $\sim 7'$ from the geometric center of the search area, with a very unusual highly polarized compact component. Finally, we present a strong radio source, EMU J062248–072246 (nicknamed Narcissus^c), which can be modeled either with a synchrotron self-absorbed spectrum or synchrotron emission from thermal electrons. It exhibits $\sim 25\%$ flux density variability over the ~ 5 -year VLASS 3 GHz survey.

Corresponding author: M. D. Filipović
m.filipovic@westernsydney.edu.au

^a) From Greek: *φαιδρα*, a Cretan princess of Greek Mythology, derived from Phaidros, Greek: *φαιδρος*, meaning 'bright'.

^b) From Greek: *Ηβη*, the Greek goddess of youth.

^c) From Greek *Ναρκισσος* was a self-absorbed hunter from Thespieae in Boeotia.

Keywords: High energy astrophysics – Neutrino astronomy – Ultra-high-energy cosmic radiation – Radio astronomy – Radio source catalogs

1. INTRODUCTION

Currently, only three astrophysical sources are confirmed as neutrino emitters: our Sun, the supernova SN 1987A, and the Galactic plane (Filipović & Tothill 2021; Icecube Collaboration et al. 2023). Other very likely neutrino emitters are the blazar TXS 0506+056 and the active galaxy NGC 1068 (IceCube Collaboration et al. 2022). Other possible neutrino origins include cosmogenic, Galactic, and extragalactic sources. Astrophysical neutrinos above GeV energies are typically produced by high-energy cosmic rays (CRs) interacting with matter or lower-energy photons, and these CRs originate from a variety of sources such as supernova remnants (SNRs), supernovas (SNs), microquasars, star-forming galaxies, gamma-ray bursts (GRBs), super massive black holes (SMBHs), and AGNs (Filipović & Tothill 2021). The observed and theorized neutrino energies differ between these sources, with SNs at the lower energies (<100 MeV; Hirata et al. 1987), followed by star-forming galaxies (100 GeV up to PeV; Bykov et al. 2015; Fang et al. 2020), SNRs (up to PeV or higher when embedded in dense star clusters; Bykov et al. 2015; Vieu & Reville 2023), extending up to AGNs (up to EeV; Rodrigues et al. 2021).

The recent KM3Net discovery on 13th February 2025 of the UHE neutrino (KM3-230213A, hereafter KM3-230213A; The KM3NeT Collaboration et al. 2025) provoked a worldwide search for its origin. The UHE neutrino’s origin was pinpointed to within 3° of RA(J2000) = $94^\circ.3$, Dec(J2000) = $-7^\circ.8$ with a 99% certainty, and to within $1^\circ.5$ with a 68% certainty. Being close to the equator, it is well-positioned for analysis by numerous radio surveys, including the Evolutionary Map of the Universe (EMU; Norris et al. 2021, Hopkins et al., submitted) and the Polarization Sky Survey of the Universe’s Magnetism (POSSUM; Gaensler et al. 2010, Gaensler et al., submitted) surveys, both conducted with ASKAP (Hotan et al. 2021), as well as the multi-epoch VLASS (Lacy et al. 2020) survey.

Several origins for KM3-230213A have been investigated, including Galactic, which was deemed unlikely (Adriani et al. 2025), a GRB origin (Amelino-Camelia et al. 2025), a cosmogenic origin (The KM3NeT collaboration 2025; KM3NeT Collaboration et al. 2025), and a blazar origin, specifically the well-known blazar, PMN J0606-0724, which experienced a radio flare within five days of the KM3-230213A event (KM3NeT Collaboration et al. 2025). We here present the results of a search for a potential radio-continuum counterpart of the KM3-230213A event using the ASKAP-EMU survey and the Quick-Look images from VLASS (Lacy et al. 2020). The data used in this paper are explained in Appendix A.

2. RESULTS AND DISCUSSION

2.1. Catalog generation

We use the source finding software AEGEAN (Hancock et al. 2018) to catalog ASKAP-EMU radio sources above 10σ within the 68% certainty search area. The available EMU data only covered approximately half of the 99% certainty region, and so the 68% certainty region was used. Note that part of the north-western region is not covered (Figure 1). We found 1045 radio point sources, and seven extended sources at $15''$ resolution, which we manually measured by fitting regions using the CARTA imaging software, following the methodology described in Filipović et al. (2022, 2024); Smeaton et al. (2024); Bradley et al. (2025). We estimate a 10% error for all ASKAP flux density measurements (Hopkins et al., submitted.).

We use the EMU catalog as a base to cross-match with other catalogs using a $2''$ matching radius. We calculate the spectral indices α , defined as $S \propto \nu^\alpha$ (Filipović & Tothill 2021), for all sources with more than two flux density measurements, and cross-match with redshift surveys to find distances. We calculate spectral indices for 185 sources and find cataloged redshifts for one point source (Jones et al. 2009) and three extended sources (Koribalski et al. 2004; Jones et al. 2009; Bilicki et al. 2014). A table of the documented information is provided in Appendix B.

2.2. Objects of interest

We find several objects of interest. The potential blazar counterpart, PMN J0606-0724, analyzed by KM3NeT Collaboration et al. (2025), is not discussed here as it is located outside of the EMU tile coverage.

2.2.1. Radio spectra candidates

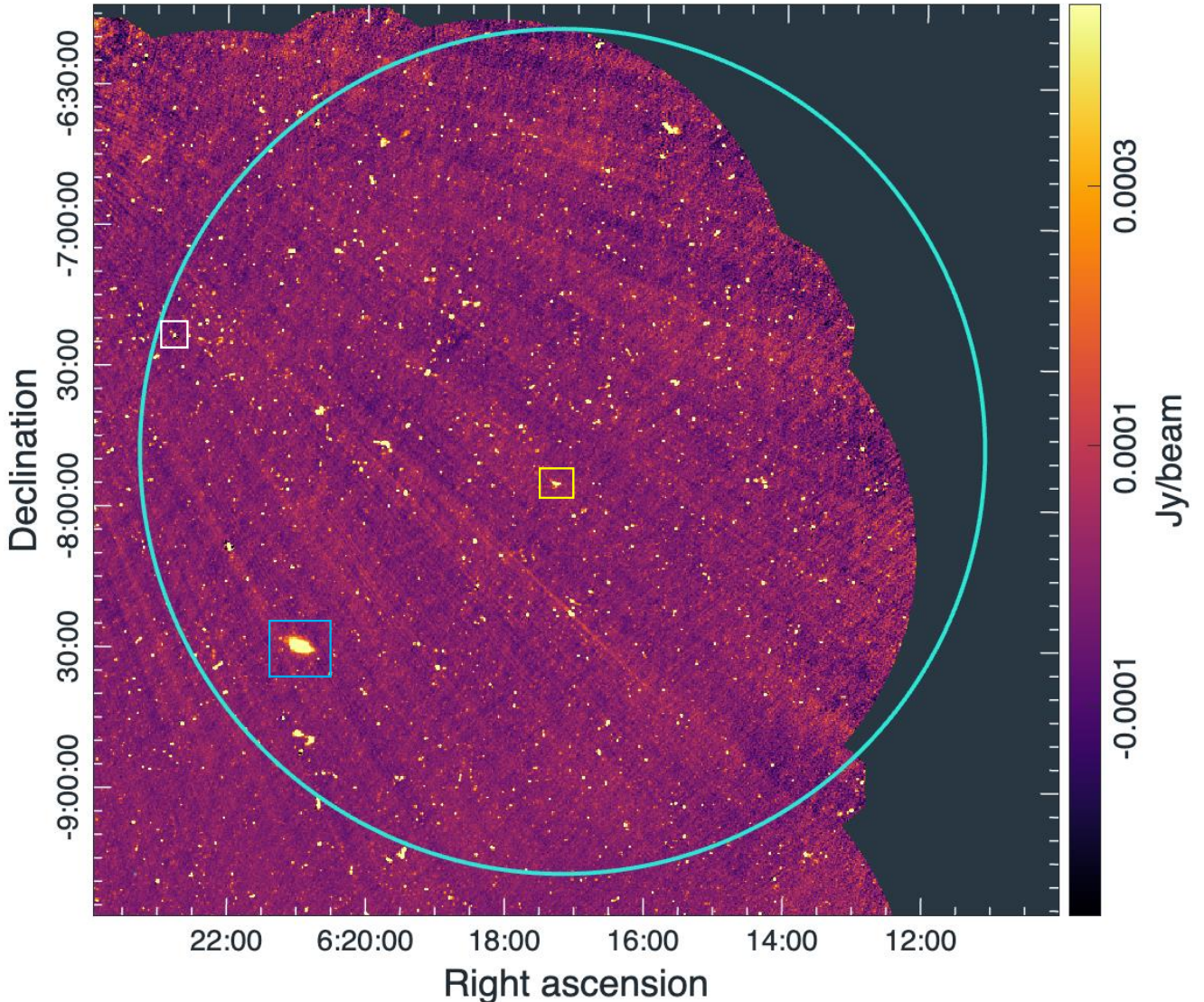


Figure 1. ASKAP 944 MHz radio continuum image, SB 59692. The cyan-colored circle (radius = $1^{\circ}5$) indicates the 68% confidence area of the neutrino event. The image is linearly scaled and has a synthesized beam of $15''$. Colored squares show the locations of three objects of interest; the white square shows the variable source Narcissus (EMU J062244–072333; see Sec. 2.2.4), the yellow square shows Hebe (WISEA J061715.89–075455.4; see Sec. 2.2.3), and the blue square shows Phaedra (UGCA 127; see Sec. 2.2.2).

We calculated spectral indices for 185 point sources with a mean value of $\alpha = -0.75 \pm 0.12$ (SD = 0.39 ± 0.15). This value and distribution match the observed average for extragalactic radio point sources (Pennock et al. 2021; Filipović et al. 2021), indicating that the sources have predominantly extragalactic origin.

Blazars are one of the expected astrophysical high-energy neutrino sources, and are typically radio-continuum variable with flat spectral indices (Filipović & Tothill 2021). We find ten blazar candidates based on their spectra, seven that exhibit a gigahertz peaked spectrum (GPS)-like spectrum (Collier et al. 2018) (EMU J061335–080331, EMU J061750–083920, EMU J061831–075415, EMU J061835–081043, EMU J061848–074327, EMU J062215–075522, and EMU J062245–072330 (see Sec. 2.2.4)), and three that exhibit possible spectral variability (EMU J061227–080810, EMU J061415–083920, and EMU J062244–072334). These blazar candidates are also possible producers of the KM3–230213A event.

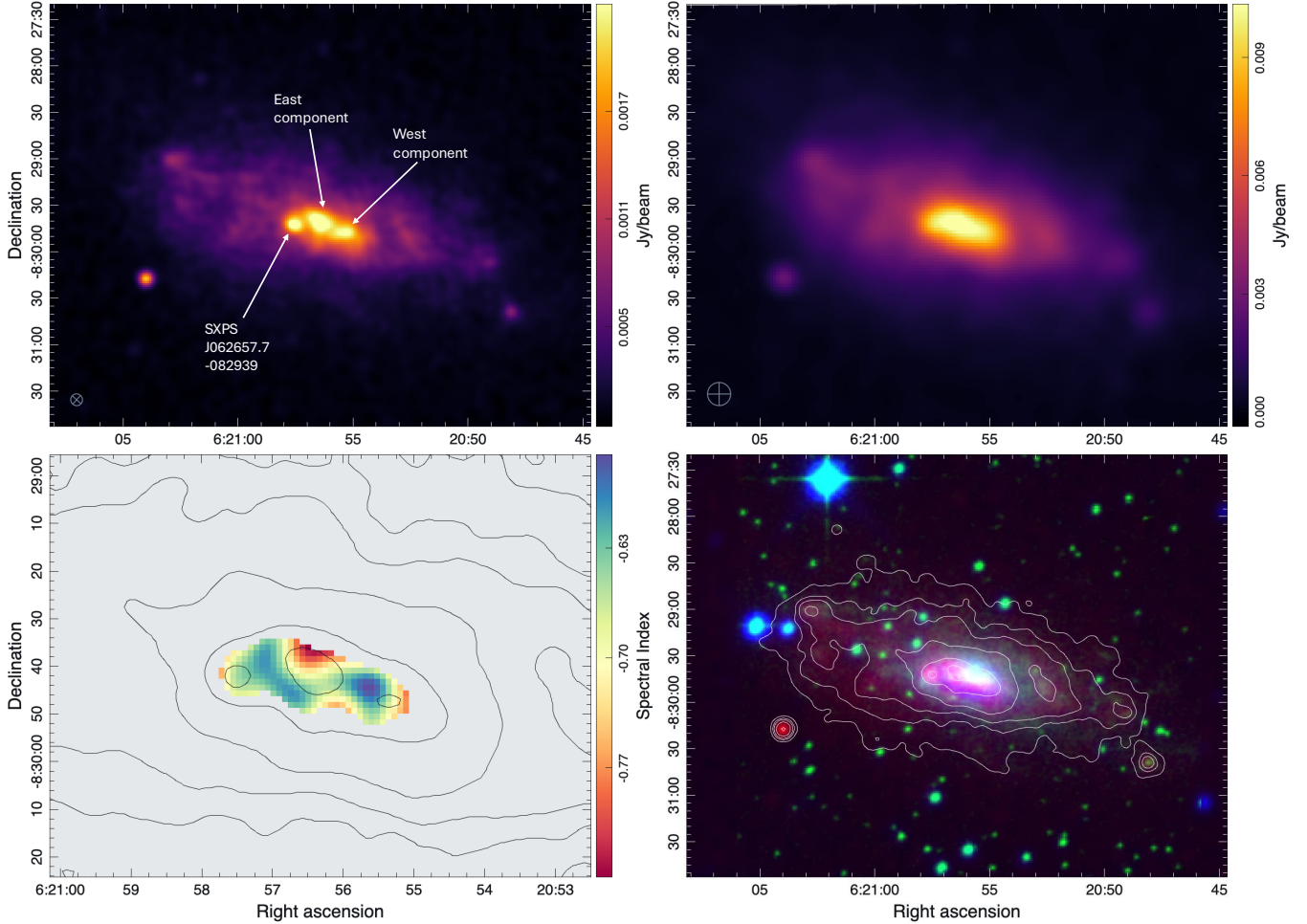


Figure 2. Multi-frequency and spectral index maps of the galaxy UGCA 127 (Phaedra). **Top left:** MeerKAT 1.3 GHz radio continuum image. The radio components to the east and west of the galaxy core and the X-ray source 2SXPS J062057.7–082939 are annotated. The synthesized beam ($7''.68 \times 7''.52$, P.A. = -40°) is shown in the bottom left corner. The image has a local RMS noise level of $\sim 15 \mu\text{Jy beam}^{-1}$. **Top right:** ASKAP 944 MHz radio continuum image. The $15''$ synthesized beam is shown in the bottom left corner. The image has a local RMS noise level of $\sim 50 \mu\text{Jy beam}^{-1}$. **Bottom left:** Spectral index map zoomed to show only the central emission. The map was generated using the high-resolution ASKAP 944 MHz image, the MeerKAT 1.3 GHz image, and the 3-epoch averaged VLASS 3 GHz image as described in Sec. 2.2.2. The final image was convolved to $10''$. **Bottom right:** Multi-frequency RGB image, consisting of MeerKAT 1.3 GHz (red), optical DSS2 R -band (green), and WISE $3.4 \mu\text{m}$ (blue) images. All images are linearly scaled, and the bottom row includes MeerKAT 1.3 GHz radio contours at levels of 10, 20, 30, 50, 100, and 150σ , where $1 \sigma = 15 \mu\text{Jy beam}^{-1}$.

2.2.2. Phaedra (UGCA 127; EMU J062056–082949)

The most prominent radio source in the field is the nearby Scd type galaxy UGCA 127 (HIPASS J0620–08, see Appendix C), with a systemic velocity of $v_{\text{sys}} = 732 \pm 2 \text{ km s}^{-1}$ (Koribalski et al. 2004) and a distance of $D = 8.3 \pm 0.6 \text{ Mpc}$. We give it the nickname Phaedra.

We measure a radio-continuum extent of $210'' \times 90''$ ($8.4 \times 3.6 \text{ kpc}$) in the ASKAP 944 MHz image (Figure 2, top-right) and detect two resolved hotspot-like features in the 1.3 GHz MeerKAT image. These indicate potential AGN jets oriented within the galaxy plane (marked East and West in Figure 2, top-left). We detect linear polarization in the POSSUM data. Unfortunately, this area is contaminated with bright, smooth Galactic foreground emission at overlapping Rotation Measure (RM)s, meaning we cannot easily separate the features, and so this polarization data is not used in this analysis. We combine our cataloged ASKAP flux densities (Appendix B) with Parkes-MIT-NRAO (PMN) (Griffith et al. 1995, $S_{4850 \text{ MHz}} = 0.084 \pm 0.011 \text{ Jy}$) and MeerKAT (Condon et al.

2021, $S_{1280\text{ MHz}} = 0.201 \pm 0.020$ Jy; B.S. = $7.68'' \times 7.52''$), and calculate an $\alpha = -0.61 \pm 0.01$ and a radio luminosity $L_{1\text{ GHz}} = 1.9 \times 10^{21}$ W Hz $^{-1}$. This indicates non-thermal emission, consistent with the presence of possible CR accelerators within Phaedra.

We generate a spectral index map with high-resolution EMU, MeerKAT, and 3-epoch averaged VLASS data using the MIRIAD (Sault et al. 1995) MATHS function. We convolve all images to a common beam size of $10'' \times 10''$ and calculate the spectral index per pixel. The VLASS image is only reliable for the inner emission due to missing short spacing, so the images were cut at a 2 mJy beam^{-1} level. We measure an average $\alpha = -0.67 \pm 0.07$ over the entire region shown (Figure 2, middle left), with the west component being the flattest $\alpha = -0.57 \pm 0.06$. This is consistent with a central engine of higher energy injection and particle acceleration in the west component.

We calculate Phaedra’s IR colors using AllWISE data (Cutri et al. 2013) as $W1 - W2 = 0.226$ and $W2 - W3 = 3.839$. Comparing with the color-color diagram of Wright et al. (2010, their Figure 12), we find Phaedra located in the region common to spiral galaxies, starburst galaxies, and luminous IR galaxies (LIRGs). Being in the starburst region indicates that Phaedra may be experiencing a starburst, potentially caused by AGN feedback, which provides another potential site of particle acceleration (Aiello et al. 2024; Marinelli et al. 2021). While we lack direct observational evidence for star-forming galaxies as UHE neutrino sources (Bechtol et al. 2017), there are numerous models which predict these areas can produce neutrinos up to PeV energies (Bykov et al. 2015).

We detect an offset between the central radio hotspots, IR and optical images, suggesting possible inner knots of a radio jet rather than the galaxy nucleus (Velović et al. 2022). If the emission is caused by jets, it may indicate areas of higher energy if the jets are oriented within the galaxy plane and thus pushing through denser material. It also suggests that the emission may instead be similar to a superbubble, (e.g. 30-Doradus C in the Large Magellanic Cloud; Kavanagh et al. 2015; Sano et al. 2017; Kavanagh et al. 2019; Yamane et al. 2021), microquasars (e.g. Galactic SS 433 or NGC 7793’s S26; Soria et al. 2010; H. E. S. S. Collaboration et al. 2024), recent core-collapse SN event(s) (Aiello et al. 2022; Ando et al. 2023), or massive star clusters (e.g. Westerlund 1; Haubner et al. 2025). All of these are areas of potential particle acceleration and CR or neutrino origin. The likely presence of dense material within the central galaxy provides a natural target for neutrino production by the CRs.

We also suggest the X-ray binary (XRB) 2SXPS J062057.7–082939 (see Figure 1 top-left; Inoue et al. 2021; Walton et al. 2022) located $\sim 25''$ from Phaedra’s center as a possible origin for KM3–230213A. This source is detected in 2SXP with an X-ray luminosity $L = 8.71 \times 10^{38}$ erg s $^{-1}$ (2–10 keV range), but is not detected in eRASS1 (Merloni et al. 2024), indicating that it is likely highly X-ray variable, as expected from an active XRB. We see a possible radio counterpart in the MeerKAT image and estimate a radio luminosity $L_{1\text{ GHz}} \sim 10^{19}$ W Hz $^{-1}$. This would make the object superluminous for an XRB radio counterpart, indicating it may be an area of UHE particle acceleration (Rhodes et al. 2022). Using the ASKAP, MeerKAT and VLASS 3-epoch combined image, we estimate a spectral index, $\alpha = -0.5 \pm 0.2$, and detect no observable variability between the three VLASS epochs. We also note three XRB candidates in Phaedra’s outer field (2SXPS J062053.1–083026, 1eRASS J062054.9–083006, 1eRASS J062047.1–083026) that have no corresponding radio emission.

Phaedra is unlikely to contain a blazar due to its steeper spectral index and lack of detected variability. However, it hosts several potential areas of UHE particle acceleration. Due to particle escape as in the commonly used “leaky box” models, the spectrum of the diffuse CRs within spiral galaxies is likely different than the CR spectra injected from the accelerators. Furthermore, reacceleration of CRs, such as for example in the so-called “espresso” model, where the CRs produced at other locations of the galaxy are reaccelerated within the jets of a central AGN engine, can also change the resulting CR distribution and contribute to the production of UHECRs (Caprioli 2015). These processes might be identified by differentiating areas of different spectral indices within a galaxy, such as done by Duric et al. (1995); Duric (2000). However, our radio data is unfortunately not of sufficiently high resolution for such a detailed spectral analysis. The proposed AGN jets are a potential origin, but they appear oriented away from us, and the star formation rate (SFR) is inconclusive. These jet orientations have been observed in other galaxies, some of which are possible high-energy neutrino sources, e.g. NGC 1068 (Padovani et al. 2024), NGC 7469 (Sommani et al. 2024), and NGC 5938 (Zakir et al. in prep). It is possible that these jets are emitting UHE-CRs into surrounding space; by interacting with ambient gas or photons, they can produce neutrinos. This raises the possibility that the neutrino direction may not point directly to the particle acceleration site.

To assess the probability of chance association of Phaedra, we used the bright galaxy number counts (Yasuda et al. 2001), which implies 0.4 galaxies with a similar or brighter magnitude in a 1.5 radius. This can mean a likely chance

association, but we note that galaxies with radio properties similar to that of Phaedra are rarer than the total number counts.

2.2.3. Hebe (WISEA J061715.89–075455.4)

The closest extended radio source to the target position is found $\sim 7'$ to its south. Called Hebe here, it is a double radio galaxy with diffuse lobes and an extraordinary slightly resolved polarized component, offset by $3''$ along the direction of its major axis from the IR galaxy WISEA J061715.89–075455.4 (see Figure 3). At a redshift of $z = 0.125 \pm 0.017$ ($D = 553.89 \pm 38.77$ pc; Bilicki et al. 2014), this offset corresponds to 8 kpc. No compact component is visible in the total intensity image, but we made a very rough estimate of its contribution by forcing a fit to a Gaussian component at that position, along with additional components for the lobes. This yielded a flux of ≈ 1.5 mJy/($18''$ beam).

The bright peak polarized intensity is 0.8 mJy beam $^{-1}$ above its local background. There is clear depolarization, consistent, e.g., with a Burn-slab model with an rms scatter of $\sim 5 \frac{\text{rad}}{\text{m}^2}$. After correction for depolarization, this corresponds to an apparent remarkable $\geq 100\%$ polarization, varying only slightly with the unknown spectral index. Even core-dominated quasars have typical fractional polarizations of only a few percent (Pushkarev et al. 2023), although the resolved components of pc-scale Very Long Baseline Interferometry (VLBI) jets can reach levels of 10s of percent (e.g., Jorstad et al. 2005). The rotation measure of the polarized peak is $59 \pm 1 \frac{\text{rad}}{\text{m}^2}$, close to the value of the local Galactic foreground, ($\approx 52 \frac{\text{rad}}{\text{m}^2}$; Hutschenreuter et al. 2022), so there is no evidence for a large, additional Faraday component local to Hebe.

At 8 kpc from the presumed AGN core in WISEA J061715.89–075455.4, Hebe’s central polarized component could also be a jet, which is only slightly resolved here, although its direction would be almost perpendicular to the more extended emission. We estimate an integrated spectral index $\alpha = -0.65 \pm 0.02$ for Hebe (see Table B), although we are not able to measure any spatial-spectral structure, especially of the polarized core.

There were four ASKAP observations of the field spanning December 11th, 2023 through April 13th, 2024, three of which were rejected because of instrumental problems. Nonetheless, we looked for variability in the peak polarized intensity and found it to be $< 10\%$. In total intensity, the quality of the data prevented any useful limits.

WISEA J061715.89–075455.4 is the northernmost member of a triplet of galaxies, which can be seen in PanSTARRS to be embedded in a common faint envelope. The envelope’s southern boundary has a curious bow shape, perhaps indicating dynamical interactions within this system.

It is unclear whether Hebe is related to the class of blazars or other core-dominated radio AGN. Blazars are of interest as possible sources of cosmic neutrinos (Albert et al. 2024), so further investigation of Hebe is warranted. One interesting model to explore for Hebe would be the “espresso” scheme (Caprioli 2015) using relativistic jets for the generation of UHECRs. Monitoring in radio polarization and searching for possible optical polarization in WISEA J061715.89–075455.4 would be especially valuable.

2.2.4. VLASS investigation and Narcissus (EMU J062248–072246)

We search for VLASS counterparts for all cataloged ASKAP sources. We then average the images from the three VLASS epochs and convolve them to the ASKAP resolution of $15''$. We record the peak flux densities as VLASS is insensitive to extended emission. We measure the spectral index between ASKAP and VLASS and find $\alpha \sim -1$ for the brightest ASKAP sources, slightly steeper than expected (Pennock et al. 2021; Cotton et al. 2024) likely due to missing VLASS flux densities, and flatter and inverted spectral indices for dimmer ASKAP sources (< 5 mJy) due to our 3σ VLASS cutoff. We find six sources with $S_{944} > 5$ mJy and $\alpha > 0$ (inverted), marked with asterisks in Appendix B, which deserve further scrutiny.

We examine the sources with the largest variability in the three VLASS epochs. The median differences between the full-resolution epoch pairs for this VLASS tile can be modeled as a noise contribution of ~ 0.2 mJy beam $^{-1}$, and a flux normalization error of $\sim 5\%$, arising from instrumental effects including incomplete cleaning. We visually examine 20 sources showing the highest fractional variability integrating the flux density in a $20''$ box. We investigate a number of sources which show significant variability.

The most obviously variable source across the VLASS epochs (2017 November 30, 2020 October 9, and 2023 March 10) is the southern source in Figure 4, (EMU J062248–072246, hereinafter Narcissus). At the native VLASS $3''$ resolution, its peak flux densities are 85.4, 70.4, and 65.2 mJy beam $^{-1}$ with errors of 0.15 mJy beam $^{-1}$. The northern source (EMU J062248–072246) also appears variable, with peak flux densities of 2.1, 3.7 and 1.3 mJy beam $^{-1}$. Both components are consistent with being unresolved within the errors. We also search within

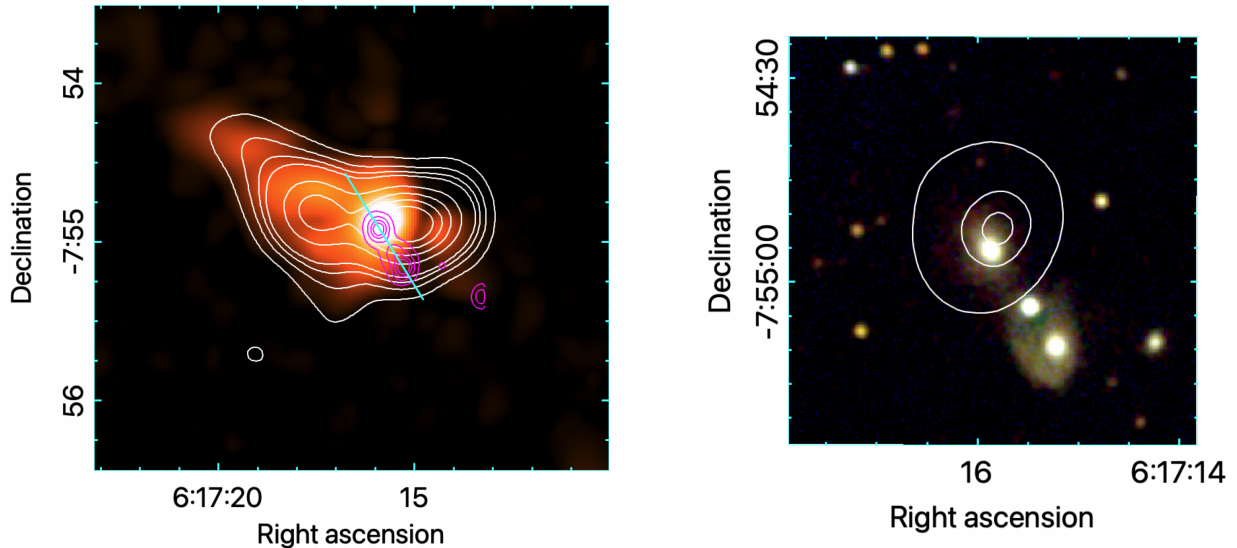


Figure 3. Left: polarized intensity of Hebe at 944 MHz, overlaid with white contours of total intensity at (0.5, 1, 1.5, 2, 4,...) mJy beam^{-1} . The cyan line indicates the orientation of the inferred magnetic field at the polarized peak after Faraday rotation correction, and the magenta contours are of the WISE W1 image. Right: PanSTARRS image, combining the z , i , and r frames, overlaid with contours of polarized intensity at 0.5, 0.8 and $0.9 \text{ mJy beam}^{-1}$. The faint optical envelope is seen, in more burned-out images, to encompass all three galaxies.

the EMU data, but detect no variability for Narcissus during the 5-hr observation. Both sources have WISE counterparts (WISEA J062244.90–072334.9 – south, and WISEA J062248.41–072247.9 – north), with colors consistent with AGNs, as expected for radio-selected samples (e.g., Wong et al. 2025). To better separate the adjacent bright WISE source in the south, we looked at the unWISE colors, which yield $W1-W2=1.3$, consistent with an AGN. Approximately 4% of compact sources at 3 GHz exhibit variability at the $\sim 30\%$ level (Mooley et al. 2016), and are expected to be associated with AGN, so these results themselves are not unusual.

What is unusual is the broadband spectra of Narcissus, when we combine 4.85 GHz data (Griffith et al. 1995) with our catalog data (Figure 4, left). We show two possible models. The first model, with the maximum possible low-frequency slope of $\alpha = +2.5$, corresponds to a compact, homogeneous source with synchrotron self-absorption. At the high, optically thin part of the spectrum, where the variability is observed, the slope is $\alpha = -0.5$, consistent with the limit for strong (non-relativistic) Fermi I shock acceleration (Filipović & Tothill 2021). Although an AGN connection for Narcissus is attractive, we cannot rule out a galactic origin. We therefore show an alternative model in Figure 4, with a low-frequency slope of $\alpha = +2$. This is similar to shock models explored by Margalit & Quataert (2024), e.g., their Fig. 3(b), used to describe explosive events such as SN1998bw and AT2018cow. Thermal absorption is another possibility for the extremely low-frequency slope.

Independent of the origins of Narcissus, Galactic or extragalactic, the steep low-frequency slope indicates that the emission is dominated by a compact, homogeneous component. This is built-in to explosive models relying on a single shock, whereas inhomogeneities, or multiple components, would broaden the spectrum and flatten the slope. However, it is not clear how the need for a compact, homogeneous source applies to Narcissus since the broadband spectra span many years of observations. Further multi-frequency monitoring and VLBI observations are necessary to separate the spectra of the short- and long-term components and to compare, e.g., to the evolutionary scenarios, e.g., of Margalit & Quataert (2021).

The third VLASS epoch was observed less than one month after the KM3–230213A event, so we conduct an additional search for variability between the VLASS epochs, independent of the ASKAP base catalog, based on an approach similar to Hajela et al. (2019) and Ross et al. (2021). We identify two variable sources with $V_S = \Delta S / \sigma_{\Delta S} > 4\sigma(V_{S,\text{population}})$ and $m = \Delta S / \bar{S} > 0.26$. The first source is the rotating variable radio star 1RXS J061542.9–072339¹ (Driessen et al.

¹ <https://radiostars.org/>

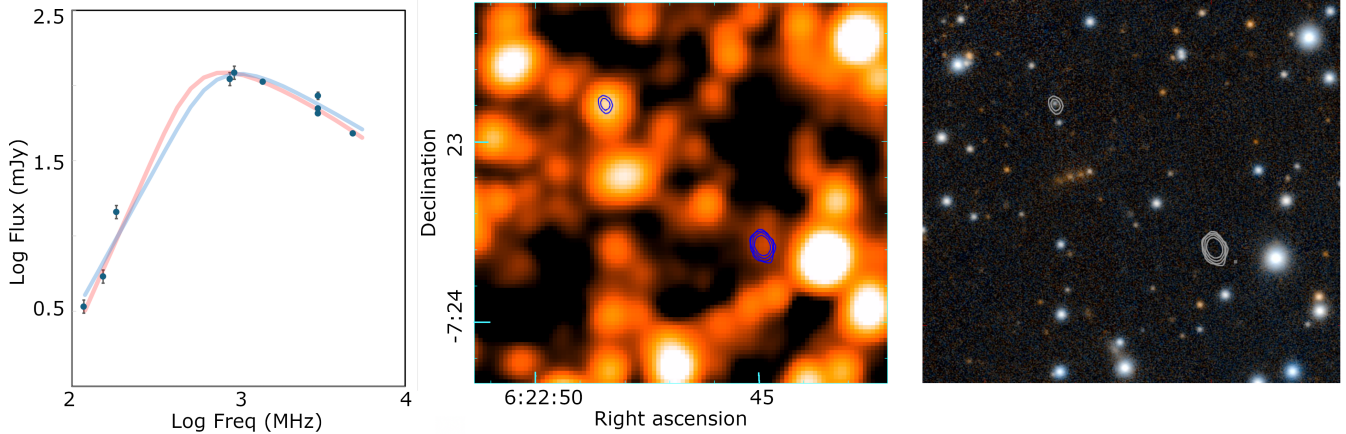


Figure 4. Left: Broadband spectrum of Narcissus (EMU J062244–072333, including minor contributions from EMU J062248–072246 low frequencies, from the larger beams). Values from all three VLASS epochs are shown. The illustrative spectra are for a homogeneous self-absorbed synchrotron source, with an optical depth of 1 at 600 MHz and an optically thin index of -0.5 (pink), and synchrotron emission from a sub-relativistic shock of *thermal* electrons at frequencies below the thermal cooling threshold, with an optically thin slope of -0.15 (blue). Middle: Overlay of the two radio sources from the VLASS map averaged over all epochs on the WISE W1 image. Right: Overlay on the multi-band PanSTARRS image.

2024) which brightens from flux densities of 2.4 ± 0.3 and 2.1 ± 0.3 mJy in the first two epochs, to 4.9 ± 0.6 mJy in the third epoch. The second source is the AGN, WISEA J062248.41–072247.9, which has flux densities of 2.1 ± 0.3 , 3.7 ± 0.4 and 1.4 ± 0.2 mJy, in the three VLASS epochs, respectively. Its radio variability and the quasar-like IR colors are consistent with blazars, which are known neutrino emitters (IceCube Collaboration et al. 2018).

2.2.5. VAST investigation

The KM3–230213A event is covered by the ASKAP Variables and Slow Transients (VAST) extragalactic survey (Murphy et al. 2021). The survey began in June 2023 and covers $\sim 10,000$ deg² at a central frequency of 888 MHz to a noise level of $250 \mu\text{Jy}$ approximately every two months.

We queried the VAST transient detection pipeline (Stewart et al. 2024b) for sources within the localization region using VAST-TOOLS (Stewart et al. 2024a). We applied standard quality cuts to remove artifacts, requiring the nearest neighbor to be separated by $> 15''$; a peak-integrated flux ratio of < 1.4 and at least one detection with an S/N greater than seven. 44 sources satisfy these criteria, but after manually inspecting all light curves, none exhibit sufficient variability to be associated with the neutrino event.

Separately, we have searched for variability from the two EMU sources (shown in Figure 4) of interest reported in this work. EMU J062248–072246 is not detected in our survey, which is not surprising given the relative sensitivity. EMU J062244–072333 is detected in all 10 observations which cover it, with a typical integrated flux density of ~ 110 mJy. It exhibits minimal variability, with a modulation index of 8% across the observation, and no obvious trends, with any intrinsic variability inseparable from stochastic variability induced by refractive interstellar scintillation.

3. CONCLUSION

We catalog ASKAP and VLASS radio sources in the 68% confidence region of the UHE neutrino event, KM3–230213A. We identify ten possible blazar candidates in the field that could produce UHE neutrinos. We further analyze three individual objects, the nearby spiral galaxy UGCA 127 (Phaedra), the radio galaxy (Hebe) closest to the geometric search area center and an unusual compact radio source (Narcissus). Phaedra is the most prominent radio source in the field and is a star-forming galaxy. However, jets may be interacting with the galaxy plane itself, causing starburst regions. This possibility, as well as that of SNRs and microquasars within the galaxy, and the well-known XRB, provide areas of possible neutrino generation within Phaedra. Hebe contains an unusual, very highly polarized compact component, likely associated with one of a triplet of galaxies in a common envelope. Narcissus is a radio source that displays radio variability in VLASS, originating in a compact, heavily absorbed AGN or a more local explosive event. These properties are consistent with known neutrino producers, making Narcissus a plausible candidate for the neutrino origin. Both Hebe and Narcissus are clearly associated with an explosive activity that could produce UHE

neutrinos, making them the most likely candidates. Phaedra shows evidence of more high-energy emission than other galaxies, making it a possible candidate, albeit this evidence is somewhat weaker than for the others. All of these systems deserve further investigation as possible origins for KM3–230213A.

4. ACKNOWLEDGMENTS

This scientific work uses data obtained from Inyarrimanha Ilgari Bundara / the Murchison Radio-astronomy Observatory. We acknowledge the Wajarri Yamaji People as the Traditional Owners and native title holders of the Observatory site. The Australian Commonwealth Scientific and Industrial Research Organisation (CSIRO)’s ASKAP radio telescope is part of the Australia Telescope National Facility². Operation of ASKAP is funded by the Australian Government with support from the National Collaborative Research Infrastructure Strategy. ASKAP uses the resources of the Pawsey Supercomputing Research Centre. Establishment of ASKAP, Inyarrimanha Ilgari Bundara, the CSIRO Murchison Radio-astronomy Observatory and the Pawsey Supercomputing Research Centre are initiatives of the Australian Government, with support from the Government of Western Australia and the Science and Industry Endowment Fund. The MeerKAT telescope is operated by the South African Radio Astronomy Observatory, which is a facility of the National Research Foundation, an agency of the Department of Science and Innovation. We thank C.W. James for discussion relating to the origin of the neutrino event and Yuri Y. Kovalev for the radio-continuum discussion. This research was funded in part by the National Science Centre, Poland, grant Nos.2018/30/E/ST9/00208 and 2023/49/B/ST9/00066. This research was supported by the Sydney Informatics Hub (SIH), a core research facility at the University of Sydney. This work was also supported by software support resources awarded under the Astronomy Data and Computing Services (ADACS) Merit Allocation Program. ADACS is funded from the Astronomy National Collaborative Research Infrastructure Strategy (NCRIS) allocation provided by the Australian Government and managed by Astronomy Australia Limited (AAL). We thank an anonymous referee for excellent comments and suggestions, which greatly improved this paper.

5. DATA AVAILABILITY

The ASKAP-EMU data used in this work are available through the CSIRO ASKAP Science Data Archive (CASDA) (<https://data.csiro.au/domain/casdaObservation>). The full table of ASKAP EMU sources generated for this paper will be made available on Vizier (<https://vizier.cds.unistra.fr/viz-bin/VizieR>) upon submission.

REFERENCES

- Adriani, O., Aiello, S., Albert, A., et al. 2025, arXiv e-prints, arXiv:2502.08387.
<https://arxiv.org/abs/2502.08387>
- Aiello, S., Albert, A., Alshamsi, M., et al. 2022, *European Physical Journal C*, 82, 317,
 doi: [10.1140/epjc/s10052-022-10137-y](https://doi.org/10.1140/epjc/s10052-022-10137-y)
- . 2024, *Astroparticle Physics*, 162, 102990,
 doi: [10.1016/j.astropartphys.2024.102990](https://doi.org/10.1016/j.astropartphys.2024.102990)
- Albert, A., Alves, S., André, M., et al. 2024, *ApJ*, 964, 3,
 doi: [10.3847/1538-4357/ad1f5b](https://doi.org/10.3847/1538-4357/ad1f5b)
- Amelino-Camelia, G., D’Amico, G., Fabiano, G., et al. 2025, On testing in-vacuo dispersion with the most energetic neutrinos: KM3-230213A case study.
<https://arxiv.org/abs/2502.13093>
- Ando, S., Ekanger, N., Horiuchi, S., & Koshio, Y. 2023, *Proceedings of the Japan Academy, Series B*, 99, 460,
 doi: [10.2183/pjab.99.026](https://doi.org/10.2183/pjab.99.026)
- Ball, B. D., Kothes, R., Rosolowsky, E., et al. 2023, *MNRAS*, 524, 1396, doi: [10.1093/mnras/stad1953](https://doi.org/10.1093/mnras/stad1953)
- Bechtol, K., Ahlers, M., Di Mauro, M., Ajello, M., & Vandenbroucke, J. 2017, *ApJ*, 836, 47,
 doi: [10.3847/1538-4357/836/1/47](https://doi.org/10.3847/1538-4357/836/1/47)
- Bilicki, M., Jarrett, T. H., Peacock, J. A., Cluver, M. E., & Steward, L. 2014, *ApJS*, 210, 9,
 doi: [10.1088/0067-0049/210/1/9](https://doi.org/10.1088/0067-0049/210/1/9)
- Bradley, A. C., Smeaton, Z. J., Tothill, N. F. H., et al. 2025, *PASA*, e032, doi: [10.1017/pasa.2025.15](https://doi.org/10.1017/pasa.2025.15)
- Bykov, A. M., Ellison, D. C., Gladilin, P. E., & Osipov, S. M. 2015, *MNRAS*, 453, 113,
 doi: [10.1093/mnras/stv1606](https://doi.org/10.1093/mnras/stv1606)
- Caprioli, D. 2015, *ApJL*, 811, L38,
 doi: [10.1088/2041-8205/811/2/L38](https://doi.org/10.1088/2041-8205/811/2/L38)
- Collier, J. D., Tingay, S. J., Callingham, J. R., et al. 2018, *MNRAS*, 477, 578, doi: [10.1093/mnras/sty564](https://doi.org/10.1093/mnras/sty564)
- Condon, J. J., Cotton, W. D., Greisen, E. W., et al. 1998, *AJ*, 115, 1693, doi: [10.1086/300337](https://doi.org/10.1086/300337)

² <https://ror.org/05qajvd42>

- Condon, J. J., Cotton, W. D., Jarrett, T., et al. 2021, *ApJS*, 257, 35, doi: [10.3847/1538-4365/ac1f17](https://doi.org/10.3847/1538-4365/ac1f17)
- Cotton, W. D., Filipović, M. D., Camilo, F., et al. 2024, *MNRAS*, 529, 2443, doi: [10.1093/mnras/stae277](https://doi.org/10.1093/mnras/stae277)
- Cutri, R. M., Wright, E. L., Conrow, T., et al. 2013, Explanatory Supplement to the AllWISE Data Release Products, Explanatory Supplement to the AllWISE Data Release Products, by R. M. Cutri et al.
- Driessen, L. N., Pritchard, J., Murphy, T., et al. 2024, *PASA*, 41, e084, doi: [10.1017/pasa.2024.72](https://doi.org/10.1017/pasa.2024.72)
- Duric, N. 2000, in *Proceedings 232. WE-Heraeus Seminar*, ed. E. M. Berkhuijsen, R. Beck, & R. A. M. Walterbos, 179–186
- Duric, N., Gordon, S. M., Goss, W. M., Viallefond, F., & Lacey, C. 1995, *ApJ*, 445, 173, doi: [10.1086/175683](https://doi.org/10.1086/175683)
- Fang, K., Banerjee, A., Charles, E., & Omori, Y. 2020, *ApJ*, 894, 112, doi: [10.3847/1538-4357/ab8561](https://doi.org/10.3847/1538-4357/ab8561)
- Filipović, M. D., & Tothill, N. F. H. 2021, *Principles of Multimessenger Astronomy*, 2514-3433 (IOP Publishing), doi: [10.1088/2514-3433/ac087e](https://doi.org/10.1088/2514-3433/ac087e)
- Filipović, M. D., Bojičić, I. S., Grieve, K. R., et al. 2021, *MNRAS*, 507, 2885, doi: [10.1093/mnras/stab2249](https://doi.org/10.1093/mnras/stab2249)
- Filipović, M. D., Payne, J. L., Alsaberi, R. Z. E., et al. 2022, *MNRAS*, 512, 265, doi: [10.1093/mnras/stac210](https://doi.org/10.1093/mnras/stac210)
- Filipović, M. D., Lazarević, S., Araya, M., et al. 2024, *PASA*, 41, e112, doi: [10.1017/pasa.2024.93](https://doi.org/10.1017/pasa.2024.93)
- Filipović, M. D., & Tothill, N. F. H., eds. 2021, *Multimessenger Astronomy in Practice* (IOP Publishing)
- Gaensler, B. M., Landecker, T. L., Taylor, A. R., & POSSUM Collaboration. 2010, in *American Astronomical Society Meeting Abstracts*, Vol. 215, American Astronomical Society Meeting Abstracts #215, 470.13
- Gordon, Y. A., Boyce, M. M., O’Dea, C. P., et al. 2021, *ApJS*, 255, 30, doi: [10.3847/1538-4365/ac05c0](https://doi.org/10.3847/1538-4365/ac05c0)
- Griffith, M. R., Wright, A. E., Burke, B. F., & Ekers, R. D. 1995, *ApJS*, 97, 347, doi: [10.1086/192146](https://doi.org/10.1086/192146)
- Guzman, J., Whiting, M., Voronkov, M., et al. 2019, ASKAPsoft: ASKAP science data processor software, *Astrophysics Source Code Library*, record ascl:1912.003
- H. E. S. S. Collaboration, Aharonian, F., Ait Benkhali, F., et al. 2024, *Science*, 383, 402, doi: [10.1126/science.adi2048](https://doi.org/10.1126/science.adi2048)
- Hajela, A., Mooley, K. P., Intema, H. T., & Frail, D. A. 2019, *MNRAS*, 490, 4898, doi: [10.1093/mnras/stz2918](https://doi.org/10.1093/mnras/stz2918)
- Hale, C. L., McConnell, D., Thomson, A. J. M., et al. 2021, *PASA*, 38, e058, doi: [10.1017/pasa.2021.47](https://doi.org/10.1017/pasa.2021.47)
- Hancock, P. J., Trott, C. M., & Hurley-Walker, N. 2018, *PASA*, 35, e011, doi: [10.1017/pasa.2018.3](https://doi.org/10.1017/pasa.2018.3)
- Harvey-Smith, L., Gaensler, B. M., Kothes, R., et al. 2010, *ApJ*, 712, 1157, doi: [10.1088/0004-637X/712/2/1157](https://doi.org/10.1088/0004-637X/712/2/1157)
- Haubner, K., Sasaki, M., Mitchell, A., et al. 2025, arXiv e-prints, arXiv:2501.12990, doi: [10.48550/arXiv.2501.12990](https://doi.org/10.48550/arXiv.2501.12990)
- Hirata, K., Kajita, T., Koshiba, M., et al. 1987, *PhRvL*, 58, 1490, doi: [10.1103/PhysRevLett.58.1490](https://doi.org/10.1103/PhysRevLett.58.1490)
- Hotan, A. W., Bunton, J. D., Chippendale, A. P., et al. 2021, *PASA*, 38, e009
- Hutschenreuter, S., Anderson, C. S., Betti, S., et al. 2022, *A&A*, 657, A43, doi: [10.1051/0004-6361/202140486](https://doi.org/10.1051/0004-6361/202140486)
- IceCube Collaboration, Aartsen, M. G., Ackermann, M., et al. 2018, *Science*, 361, eaat1378, doi: [10.1126/science.aat1378](https://doi.org/10.1126/science.aat1378)
- IceCube Collaboration, Abbasi, R., Ackermann, M., et al. 2022, *Science*, 378, 538, doi: [10.1126/science.abg3395](https://doi.org/10.1126/science.abg3395)
- Icecube Collaboration, Abbasi, R., Ackermann, M., et al. 2023, *Science*, 380, 1338, doi: [10.1126/science.adc9818](https://doi.org/10.1126/science.adc9818)
- Inoue, Y., Yabe, K., & Ueda, Y. 2021, *PASJ*, 73, 1315, doi: [10.1093/pasj/psab077](https://doi.org/10.1093/pasj/psab077)
- Jones, D. H., Read, M. A., Saunders, W., et al. 2009, *MNRAS*, 399, 683, doi: [10.1111/j.1365-2966.2009.15338.x](https://doi.org/10.1111/j.1365-2966.2009.15338.x)
- Jorstad, S. G., Marscher, A. P., Lister, M. L., et al. 2005, *AJ*, 130, 1418, doi: [10.1086/444593](https://doi.org/10.1086/444593)
- Kavanagh, P. J., Sasaki, M., Bozzetto, L. M., et al. 2015, *A&A*, 573, A73, doi: [10.1051/0004-6361/201424354](https://doi.org/10.1051/0004-6361/201424354)
- Kavanagh, P. J., Vink, J., Sasaki, M., et al. 2019, *A&A*, 621, A138, doi: [10.1051/0004-6361/201833659](https://doi.org/10.1051/0004-6361/201833659)
- KM3NeT Collaboration, MessMapp Group, Fermi-LAT Collaboration, et al. 2025, arXiv e-prints, arXiv:2502.08484, doi: [10.48550/arXiv.2502.08484](https://doi.org/10.48550/arXiv.2502.08484)
- Koribalski, B. S., Staveley-Smith, L., Kilborn, V. A., et al. 2004, *AJ*, 128, 16, doi: [10.1086/421744](https://doi.org/10.1086/421744)
- Lacy, M., Baum, S. A., Chandler, C. J., et al. 2020, *PASP*, 132, 035001, doi: [10.1088/1538-3873/ab63eb](https://doi.org/10.1088/1538-3873/ab63eb)
- Margalit, B., & Quataert, E. 2021, *ApJL*, 923, L14, doi: [10.3847/2041-8213/ac3d97](https://doi.org/10.3847/2041-8213/ac3d97)
- . 2024, *ApJ*, 977, 134, doi: [10.3847/1538-4357/ad8b47](https://doi.org/10.3847/1538-4357/ad8b47)
- Marinelli, A., Ambrosone, A., Ibsalikh, W. I., et al. 2021, *Journal of Instrumentation*, 16, C12016, doi: [10.1088/1748-0221/16/12/C12016](https://doi.org/10.1088/1748-0221/16/12/C12016)
- Merloni, A., Lamer, G., Liu, T., et al. 2024, *A&A*, 682, A34, doi: [10.1051/0004-6361/202347165](https://doi.org/10.1051/0004-6361/202347165)
- Mooley, K. P., Hallinan, G., Bourke, S., et al. 2016, *ApJ*, 818, 105, doi: [10.3847/0004-637X/818/2/105](https://doi.org/10.3847/0004-637X/818/2/105)
- Murphy, T., Chatterjee, S., Kaplan, D. L., et al. 2013, *PASA*, 30, e006, doi: [10.1017/pasa.2012.006](https://doi.org/10.1017/pasa.2012.006)
- Murphy, T., Kaplan, D. L., Stewart, A. J., et al. 2021, *PASA*, 38, e054, doi: [10.1017/pasa.2021.44](https://doi.org/10.1017/pasa.2021.44)
- Norris, R. P., Marvil, J., Collier, J. D., et al. 2021, *PASA*, 38, e046

- Padovani, P., Resconi, E., Ajello, M., et al. 2024, *Nature Astronomy*, 8, 1077, doi: [10.1038/s41550-024-02339-z](https://doi.org/10.1038/s41550-024-02339-z)
- Pennock, C. M., van Loon, J. T., Filipović, M. D., et al. 2021, *MNRAS*, 506, 3540, doi: [10.1093/mnras/stab1858](https://doi.org/10.1093/mnras/stab1858)
- Pushkarev, A. B., Aller, H. D., Aller, M. F., et al. 2023, *MNRAS*, 520, 6053, doi: [10.1093/mnras/stad525](https://doi.org/10.1093/mnras/stad525)
- Rhodes, L., Fender, R. P., Motta, S., et al. 2022, *MNRAS*, 513, 2708, doi: [10.1093/mnras/stac954](https://doi.org/10.1093/mnras/stac954)
- Rodrigues, X., Heinze, J., Palladino, A., van Vliet, A., & Winter, W. 2021, *PhRvL*, 126, 191101, doi: [10.1103/PhysRevLett.126.191101](https://doi.org/10.1103/PhysRevLett.126.191101)
- Ross, K., Callingham, J. R., Hurley-Walker, N., et al. 2021, *MNRAS*, 501, 6139, doi: [10.1093/mnras/staa3795](https://doi.org/10.1093/mnras/staa3795)
- Ross, K., Hurley-Walker, N., Galvin, T. J., et al. 2024, *PASA*, 41, e054, doi: [10.1017/pasa.2024.57](https://doi.org/10.1017/pasa.2024.57)
- Sano, H., Yamane, Y., Voisin, F., et al. 2017, *ApJ*, 843, 61, doi: [10.3847/1538-4357/aa73e0](https://doi.org/10.3847/1538-4357/aa73e0)
- Sault, R. J., Teuben, P. J., & Wright, M. C. H. 1995, in *Astronomical Society of the Pacific Conference Series*, Vol. 77, *Astronomical Data Analysis Software and Systems IV*, ed. R. A. Shaw, H. E. Payne, & J. J. E. Hayes, 433, doi: [10.48550/arXiv.astro-ph/0612759](https://doi.org/10.48550/arXiv.astro-ph/0612759)
- Smeaton, Z. J., Filipović, M. D., Lazarević, S., et al. 2024, *MNRAS*, 534, 2918, doi: [10.1093/mnras/stae2237](https://doi.org/10.1093/mnras/stae2237)
- Sommani, G., Franckowiak, A., Lincetto, M., & Dettmar, R.-J. 2024, arXiv e-prints, arXiv:2403.03752, doi: [10.48550/arXiv.2403.03752](https://doi.org/10.48550/arXiv.2403.03752)
- Soria, R., Pakull, M. W., Broderick, J. W., Corbel, S., & Motch, C. 2010, *MNRAS*, 409, 541, doi: [10.1111/j.1365-2966.2010.17360.x](https://doi.org/10.1111/j.1365-2966.2010.17360.x)
- Stewart, A., Dobie, D., O'Brien, A., & Kaplan, D. 2024a, askap-vast/vast-tools: v3.1.1, v3.1.1, Zenodo, doi: [10.5281/zenodo.8365236](https://doi.org/10.5281/zenodo.8365236)
- Stewart, A., Serg, O'Brien, A., et al. 2024b, askap-vast/vast-pipeline: v1.2.0, v1.2.0, Zenodo, doi: [10.5281/zenodo.13927015](https://doi.org/10.5281/zenodo.13927015)
- The KM3NeT collaboration. 2025, arXiv e-prints, arXiv:2502.08508, doi: [10.48550/arXiv.2502.08508](https://doi.org/10.48550/arXiv.2502.08508)
- The KM3NeT Collaboration, Aiello, S., Albert, A., et al. 2025, *Nature*, 638, 376, doi: [10.1038/s41586-024-08543-1](https://doi.org/10.1038/s41586-024-08543-1)
- Velović, V., Filipović, M. D., Barnes, L., et al. 2022, *MNRAS*, 516, 1865, doi: [10.1093/mnras/stac2012](https://doi.org/10.1093/mnras/stac2012)
- Vieu, T., & Reville, B. 2023, *MNRAS*, 519, 136, doi: [10.1093/mnras/stac3469](https://doi.org/10.1093/mnras/stac3469)
- Walton, D. J., Mackenzie, A. D. A., Gully, H., et al. 2022, *MNRAS*, 509, 1587, doi: [10.1093/mnras/stab3001](https://doi.org/10.1093/mnras/stab3001)
- Wang, J., Koribalski, B. S., Serra, P., et al. 2016, *MNRAS*, 460, 2143, doi: [10.1093/mnras/stw1099](https://doi.org/10.1093/mnras/stw1099)
- Wong, O. I., Garon, A. F., Alger, M. J., et al. 2025, *MNRAS*, 536, 3488, doi: [10.1093/mnras/stae2790](https://doi.org/10.1093/mnras/stae2790)
- Wright, E. L., Eisenhardt, P. R. M., Mainzer, A. K., et al. 2010, *AJ*, 140, 1868, doi: [10.1088/0004-6256/140/6/1868](https://doi.org/10.1088/0004-6256/140/6/1868)
- Yamane, Y., Sano, H., Filipović, M. D., et al. 2021, *ApJ*, 918, 36, doi: [10.3847/1538-4357/ac0adb](https://doi.org/10.3847/1538-4357/ac0adb)
- Yasuda, N., Fukugita, M., Narayanan, V. K., et al. 2001, *AJ*, 122, 1104, doi: [10.1086/322093](https://doi.org/10.1086/322093)

APPENDIX

A. DATA

A.1. *ASKAP EMU+POSSUM*

The 30 deg² ASKAP tile that includes the KM3-230213A event location was observed as part of EMU (Project Code AS201; Norris et al. 2021, Hopkins et al., submitted) and POSSUM (Project Code AS203, Gaensler et al. 2010, Gaensler et al., submitted). Two ASKAP scheduling blocks (SB 59692; tile EMU_0626 – 09A and SB 61077; EMU_0626 – 09B) cover this area and were observed on the 2nd of March 2024 and the 13th of April 2024, respectively, i.e. approximately 1 year after the KM3-230213A event. Both tiles use ASKAP’s 36 antenna array with a central frequency of 943.5 MHz, a bandwidth of 288 MHz, and a 300-minute exposure time. Only SB 59692 was used for source finding due to significant interference from a nearby source in SB 61077. However, SB 61077 was still able to be used for polarimetric analysis. The high-resolution EMU image (B.S.=10'') of SB 59692 was also used to generate the spectral index map for UGCA 127 (see Sec. 2.2.2) as the inner components could not be resolved in the convolved 15'' image.

The data were processed using the standard ASKAPSoft pipelines (Guzman et al. 2019), producing both a multi-frequency synthesis (MFS) band-averaged Stokes I image for EMU, and full Stokes I , Q , U and V frequency cubes with 1 MHz channels for POSSUM. De-rotation of Stokes Q and U were used to create Faraday spectra, with the amplitude of the peak in the spectrum taken as the polarized intensity. In Figure 1 we show the convolved EMU Stokes I radio continuum image which has a resolution of 15'' and an RMS noise sensitivity of $\sigma = 50 \mu\text{Jy beam}^{-1}$. We find no Stokes V emission within the search area. To obtain Stokes Q , U , polarized intensity (PI) and polarization angle (PA) images, we utilized the RM synthesis technique (Harvey-Smith et al. 2010). We did not use the Fourier transform method from the POSSUM pipeline but the de-rotation technique as described in Ball et al. (2023).

A.2. *Other radio catalogs*

We use several previous radio catalogs and surveys which overlap the search area to cross-match our sources and include the flux measurements in our catalog to calculate spectral indices (see Table B). We use data from the GaLactic and Extragalactic All-sky MWA eXtended (GLEAM-X) survey (Ross et al. 2024, $\nu = 72\text{--}231$ MHz; B.S. $\sim 45''$), the Rapid ASKAP Continuum Survey (RACS) (Hale et al. 2021, $\nu = 888$ MHz; B.S. = 25''), the NRAO VLA Sky Survey (NVSS) (Condon et al. 1998, $\nu = 1.4$ GHz; B.S. = 45''), and the VLASS Quick-Look epoch-averaged images (Gordon et al. 2021, ($\nu = 3$ GHz; B.S. $\sim 3''$)). Limitations for the VLASS Quick-Look images are discussed in Gordon et al. (2021). We also use the different epochs in the VLASS Quick-Look and ASKAP Variable and Slow Transients (VAST) surveys (Murphy et al. 2013, 2021) to search for variability.

As the ASKAP EMU tile does not cover the entire 68% confidence region, we only catalog sources that appear within the field of view. The entire region is analyzed with the VLASS data.

B. EXAMPLE TABLE

[1] NAME(S)	[2] RA (J2000)	[3] DEC (J2000)	[4] EMU 944 (MHz) $S \pm \Delta S$ (Jy)	[5] GLEAM W087 87 (MHz) $S \pm \Delta S$ (Jy)	[9] GLEAM W215 215 (MHz) $S \pm \Delta S$ (Jy)	[10] RACS 888 (MHz) $S \pm \Delta S$ (Jy)	[11] NVSS 1.40 (GHz) $S \pm \Delta S$ (Jy)	[12] VLASS 3.00 (GHz) $S \pm \Delta S$ (Jy)	[13] $\alpha \pm \Delta\alpha$	[14] n°	[15] z $z \pm \Delta z$
^a EMU J062056-082949 UGCA 127	06:20:56.50	-08:29:49.80	0.255±0.026	1.017±0.102	0.559±0.056	-	-	-	-0.61±0.01	7	-
Phaedra ($\phi\alpha\iota\delta\rho\alpha$)											
^a EMU J061716-075449 WISEA J061715.89-075455.4	06:17:16.50	-07:54:49.60	0.045±0.005	0.216±0.022	0.117±0.012	-	-	-	-0.65±0.02	7	0.13±0.01
Hebe (H197)											
^a EMU J062244-072333	06:22:44.90	-07:23:33.40	0.122±0.012	0.019±-0.002	0.003±0.0003	0.110±0.001	0.106±0.003	0.0828±0.0046	1.09±0.21	8	-
^a EMU J062248-072246	06:22:48.40	-07:22:46.20	0.002±0.0002	-	-	-	-	0.0034±0.0047	-	-	-
EMU J062053-084851	06:20:53.40	-08:48:51.70	0.106±0.011	-	-	-	-	0.0024±0.0007	-	-	-
EMU J062039-073935	06:20:39.90	-07:39:35.60	0.129±0.013	0.547±0.055	0.306±0.031	-	-	0.0079±0.0013	-1.10±0.16	7	0.13±0.01
EMU J061946-064201	06:19:46.40	-06:42:01.10	0.009±0.001	0.176±0.018	0.066±0.007	-	-	0.0011±0.0005	-1.46±0.08	7	-
EMU J061944-064232	06:19:44.50	-06:42:32.70	0.011±0.001	-	-	-	-	0.0006±0.0005	-	-	-
EMU J061542-063844	06:15:42.00	-06:38:44.50	0.108±0.011	0.547±0.055	0.229±0.023	-	-	0.0017±0.0010	-1.45±0.26	7	-
EMU J061931-063426	06:19:31.00	-06:34:26.50	0.002±0.0002	-	-	-	0.003±0.0005	0.0024±0.0003	-0.02±0.14	3	-
EMU J062118-073729	06:21:18.20	-07:37:29.30	0.007±0.001	-	-	-	0.004±0.0004	0.0032±0.0004	-0.65±0.29	3	-
EMU J061626-070526	06:16:26.80	-07:05:26.90	0.004±0.0004	-	-	0.003±0.0008	-	0.0019±0.0004	-0.44±0.32	3	-
EMU J061345-071315	06:13:45.10	-07:13:15.80	0.002±0.0003	-	-	0.003±0.0007	-	0.0011±0.0003	-0.76±0.11	3	-
EMU J061438-071836	06:14:38.60	-07:18:36.50	0.002±0.0002	-	-	0.003±0.001	-	0.0011±0.0004	-0.64±0.41	3	-
EMU J061346-082442	06:13:46.90	-08:24:42.80	0.002±0.0002	-	-	0.003±0.001	-	0.0014±0.0004	-0.51±0.45	3	-
EMU J061356-080149	06:13:56.50	-08:01:49.40	0.004±0.0004	-	-	0.004±0.001	-	0.0016±0.0004	-0.71±0.10	3	-
EMU J061336-081344	06:13:36.90	-08:13:44.00	0.003±0.0003	-	-	0.004±0.001	-	0.0019±0.0003	-0.42±0.17	3	-

Table 1. Example table of the final EMU catalog generated as a part of this survey. Column [1] is the EMU designation name, or additional names where applicable. Columns [2] and [3] are FK5 (J2000) RA and DEC positions for a given source. Columns from [4] to [13] are measured fluxes and their respective errors in Janskys (Jy), columns [6], [7] and [8] are not included, but are the central three GLEAM bands; W118, W154, and W185. Column [13] includes calculated spectral indices, and column [14] is the number of points used in spectral index calculations. Column [15] is redshift and its associated error, not included is column [16], which contains the bibliographical reference for provided redshifts. Also not included, column [17] indicates whether a source is extended or not. It is important to note that each column with associated errors is split into two columns in the full catalog. ^aSources discussed in this paper.

C. HI ANALYSIS OF THE GALAXY UGCA 127 (PHAEDRA)

UGCA 127 (HIPASS J0620–08) shows a symmetric double-horn HI profile (Figure 5), with a HI flux density of 250 Jy km s^{-1} and a HI mass of $4 \times 10^9 M_{\odot}$. We estimate a rotational velocity of 187 km s^{-1} , suggesting a total dynamical mass of $M_{\text{dyn}} = 1.4 \times 10^{11} M_{\odot}$ for an HI disk radius of 17 kpc (using the HI mass – size relation, Wang et al. 2016). A gas-rich companion (HIPASS J0622–07) is detected $\sim 45'$ to the north-east. Inoue et al. (2021) estimate a SFR of $0.36 M_{\odot} \text{ yr}^{-1}$ and a stellar mass of $2 \times 10^{10} M_{\odot}$.

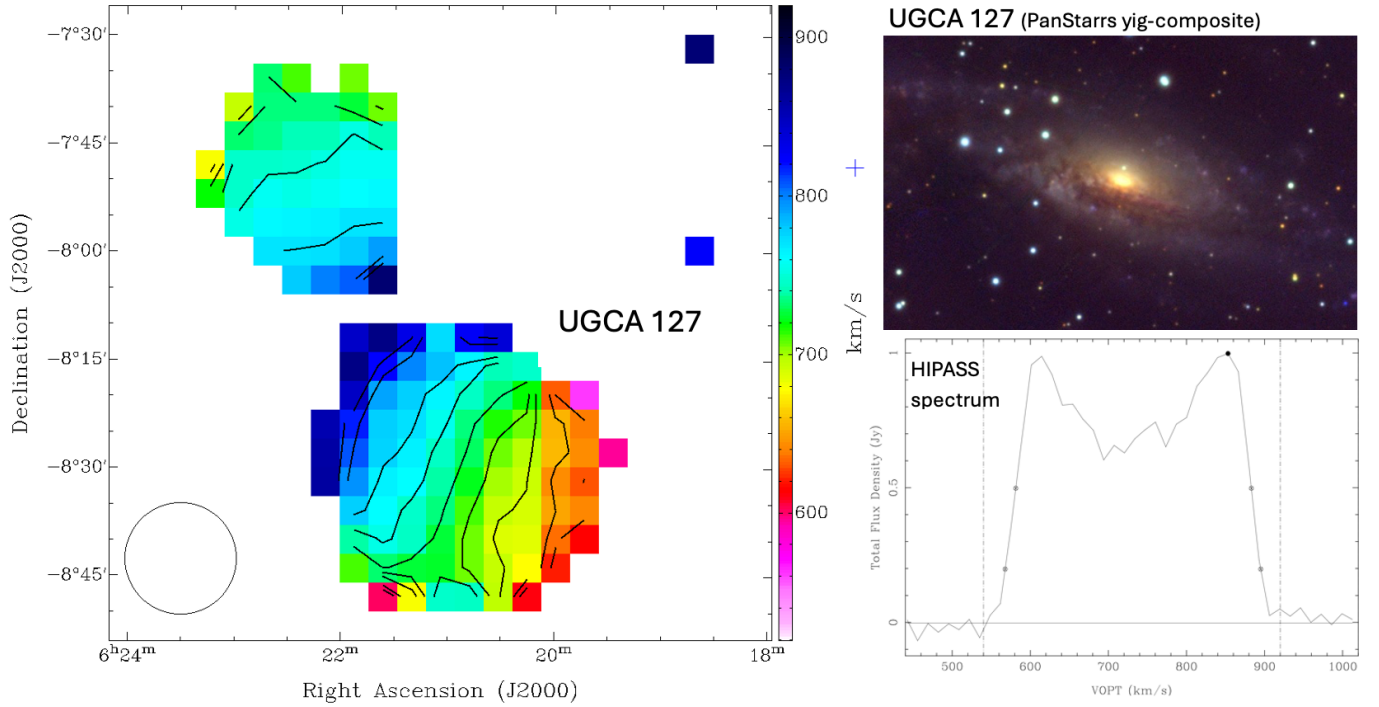


Figure 5. – **Left:** Mean HI velocity field of the galaxy UGCA 127 and its companion using data from the HI Parkes All Sky Survey (HIPASS). The Parkes gridded beam ($15.5'$) is shown in the bottom left corner. – **Top right:** PanSTARRS optical color-composite image using the *yig* bands. – **Bottom right:** Integrated HIPASS spectrum; the 50% and 20% velocity width estimates as well as the peak flux density are indicated.